united nations
educational, scientific
and cultural
organization

international atomic
energy agency

the
abdus salam
international centre for theoretical physics

SMR 1161/24

AUTUMN COLLEGE ON PLASMA PHYSICS

25 October - 19 November 1999

Turbulence Suppression with Reversed Magnetic Shear

M. BEER

Princeton University
Plasma Physics Lab.
Princeton, U.S.A.

Turbulence Suppression with Reversed Magnetic Shear

Michael A. Beer

Princeton University Plasma Physics Laboratory, Princeton, NJ 08543, USA

Autumn College on Plasma Physics
November, 1999

Acknowledgements: G. W. Hammett, W. Dorland

Outline:

- Ingredients for turbulence suppression:
  - $E \times B$ suppression of turbulence
  - Shafranov shift suppression of TEM
- Analyze examples from TFTR + JET
  - formation of internal transport barriers
- Inclusion of $E \times B$ flows in flux tube simulations

Brief Summary of ERS Experimental Results

[Levinton, et al., PRL 1995]

- ERS characterized by sudden transition to improved confinement
- Two nearly identical shots, slightly higher P_{beam} transitioned
- After transition, core n_e rises linearly in time

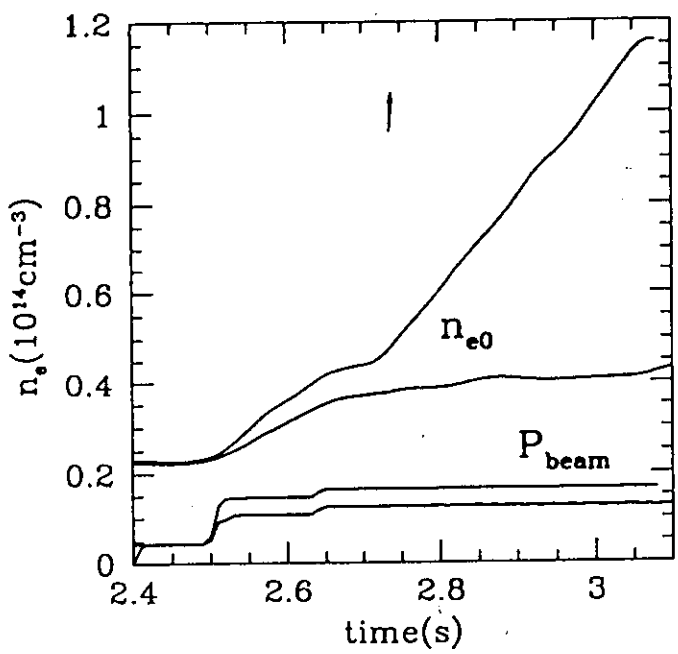

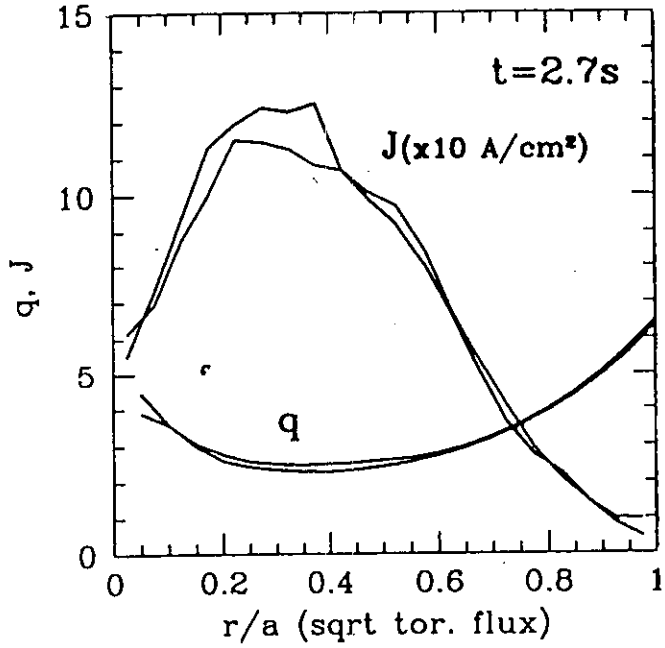

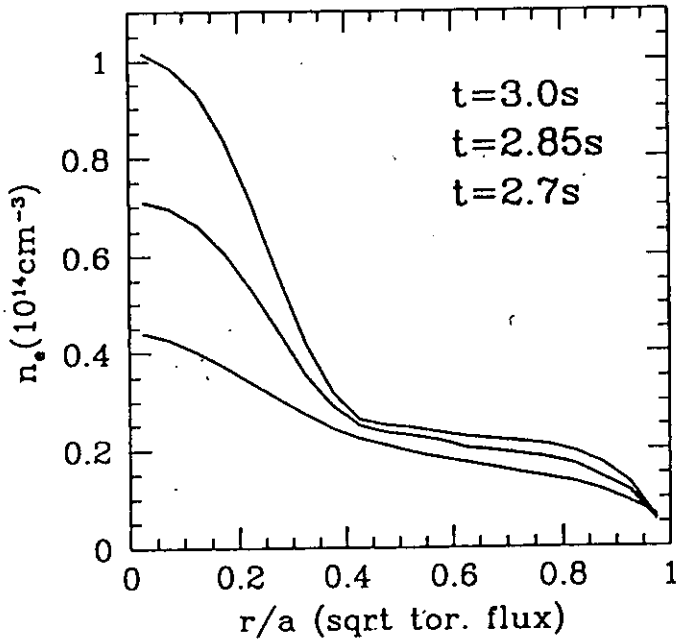

Linear ERS Results

Linear Eigenfrequencies for TFTR ERS Shot #84011 at $t = 3$s with D+C+beams+trapped electrons, maximized over $k_\theta \rho_i$:

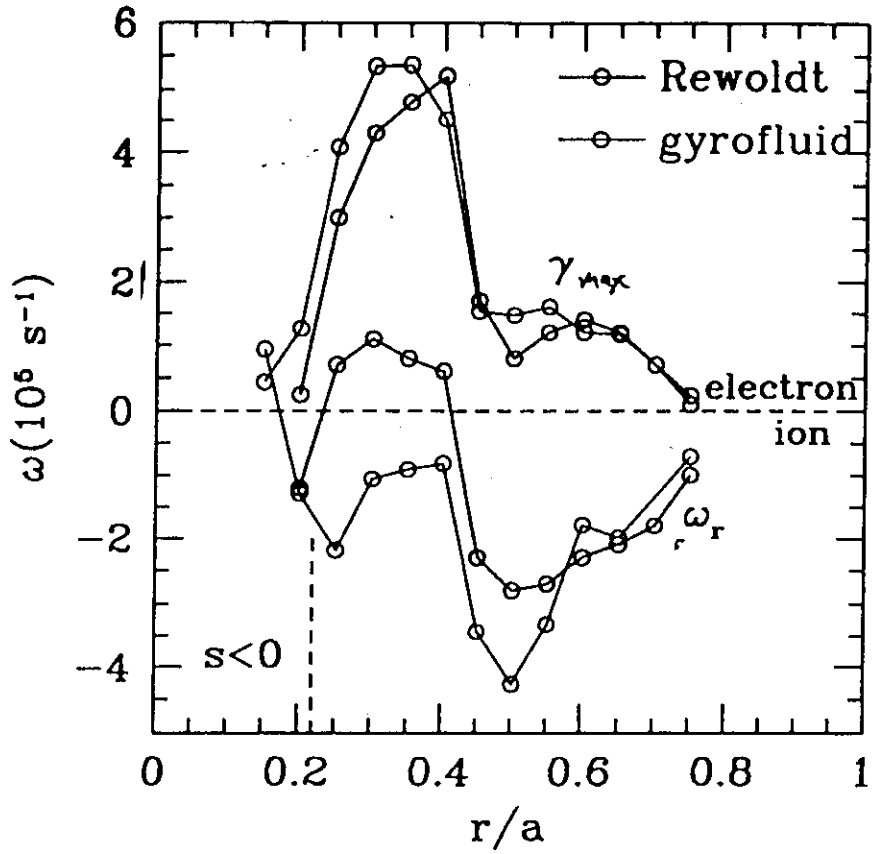

Both calculations use general magnetic geometry
Rewoldt: slowing-down beam
Gyrofluid: **Maxwellian** beam

- **high-k_θ TEM** dominant instability in core, $r/a < 0.4$
- lower-k_θ **ITG** dominant for $r/a > 0.4$
- ITG stable in core: steep $\nabla n_i \Rightarrow$ low η_i

Longest wavelengths stabilized at transition

Linear TEM growth rates for ERS #84011, $r = .24a$.

Transition at $t = 2.71$s.

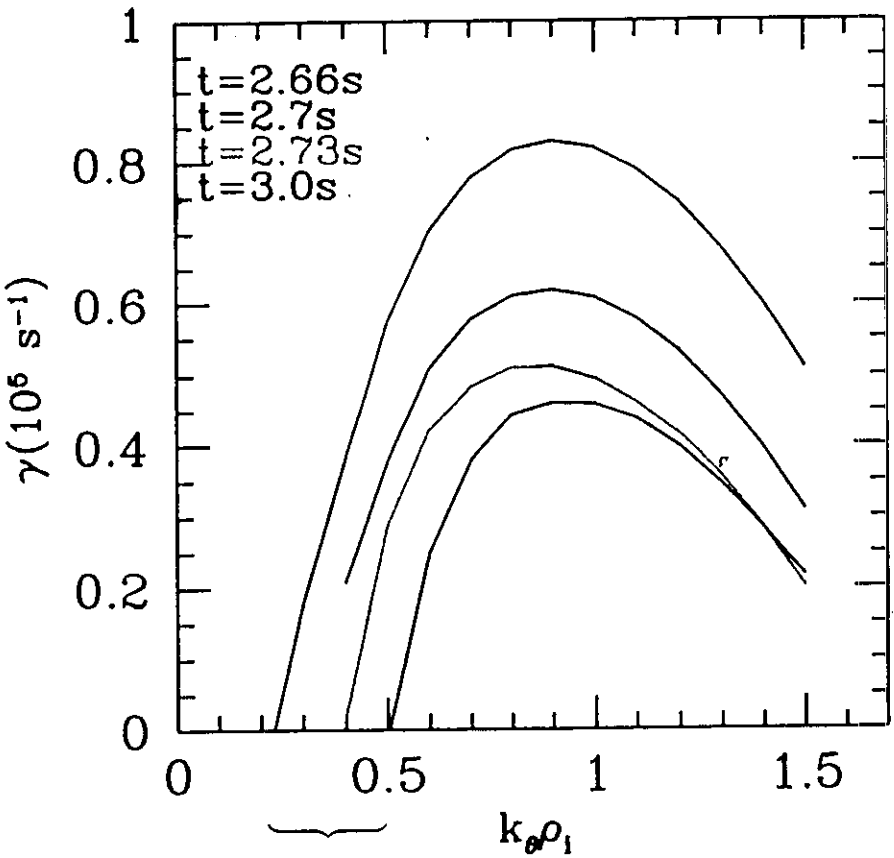

Longest wavelengths stabilized at transition. Because the large scales cause more transport, transport drops significantly, as will be seen from nonlinear simulations.

Pitch Angle Dependence of Toroidal Precession Drift

Both $\hat{s} < 0$ and $\alpha = -q^2 R d\beta/dr > 0$ cause favorable precession of all but deeply trapped electrons and can stabilize TEM.

Finite-β drift reversal first pointed out by [**Rosenbluth & Sloan, PF 1971**].

Also investigated in [**Newberger, Ph.D. thesis, Princeton (1976)**].

$$\begin{aligned}\langle \omega_{de} \rangle_b(\kappa) &= \frac{k_\theta \rho_e v_{te}}{R} \langle \cos\theta + (\hat{s}\theta - \alpha \sin\theta) \sin\theta \rangle_b \\ &= \frac{k_\theta \rho_e v_{te}}{R} \left[G_0(\kappa) + \hat{s} G_s(\kappa) + \alpha G_\alpha(\kappa) \right]\end{aligned}$$

where

$$G_0(\kappa) = 2\frac{E(\kappa^2)}{K(\kappa^2)} - 1$$

$$G_s(\kappa) = 4\left(\frac{E(\kappa^2)}{K(\kappa^2)} + \kappa^2 - 1\right)$$

$$G_\alpha(\kappa) = \frac{4}{3}\left(\frac{E(\kappa^2)}{K(\kappa^2)}(1 - 2\kappa^2) + \kappa^2 - 1\right)$$

Pitch angle dependence of terms in precession frequency

$$\langle \omega_{de} \rangle_b (\kappa) = \frac{k_\theta \rho_e v_{te}}{R} \left[G_0(\kappa) + \hat{s} G_s(\kappa) + \alpha G_\alpha(\kappa) \right]$$

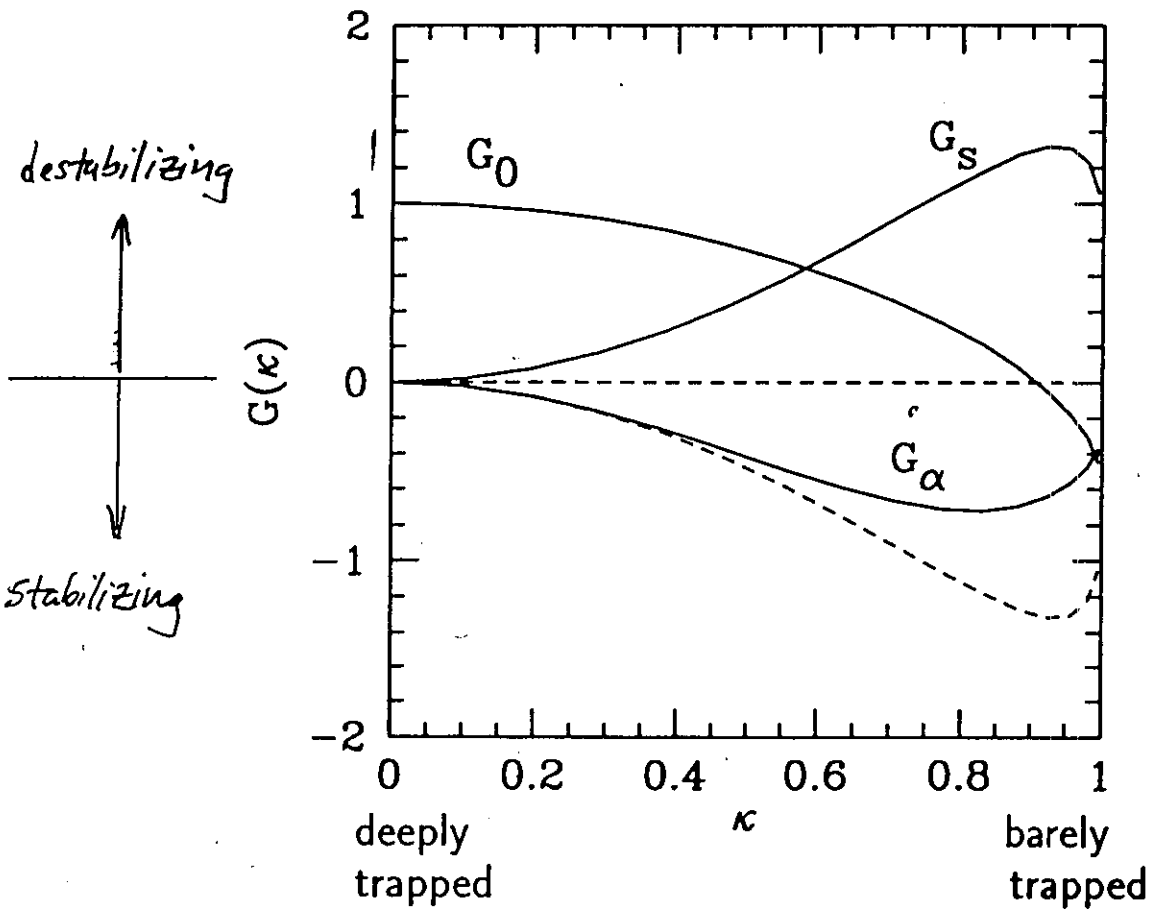

For TFTR ERS core parameters, **Shafranov shift induced drift reversal (α) actually** dominates:

$$\hat{s} \sim -1/4 \qquad \alpha \sim 2$$

where the core is well into the ballooning second stability regime.

Large Shafranov Shift Causes Much of Drift Reversal and TEM Suppression

Precession vs. Pitch Angle, κ

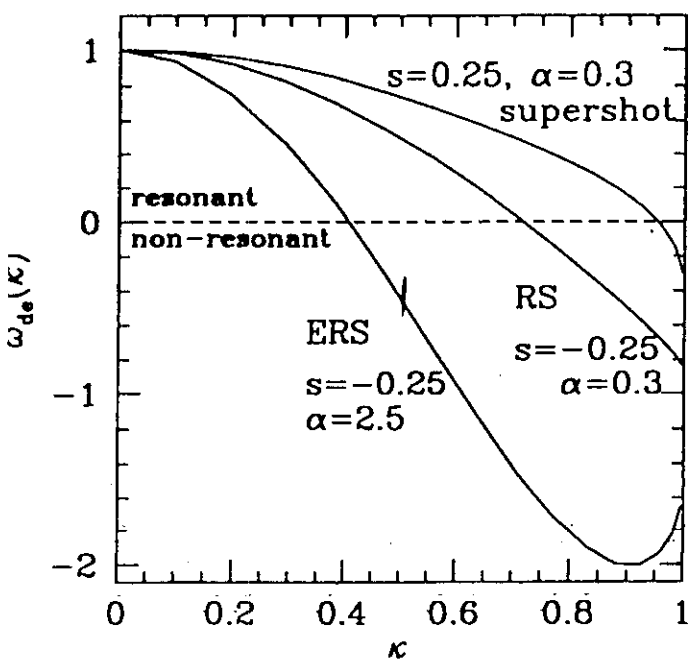

deeply trapped — barely trapped

Growth Rates

ERS 84011, r=.25a, t=3s

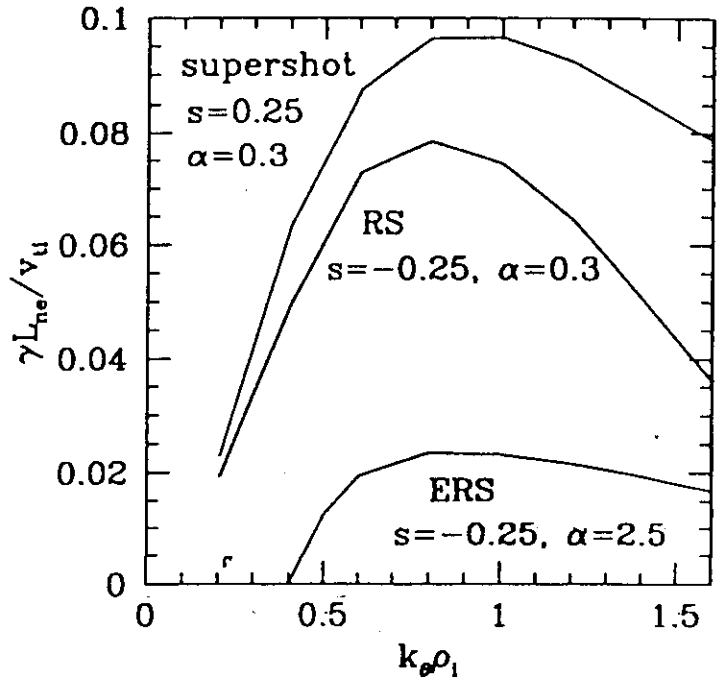

Longest wavelengths stabilized in ERS, but high-k TEM still unstable

General Geometry Enhances Drift Reversal

- Calculate equilibria (JSOLVER) using measured TFTR profiles after transition, at $t = 3.0$s
- Repeat reducing all densities by 10

Actual profiles

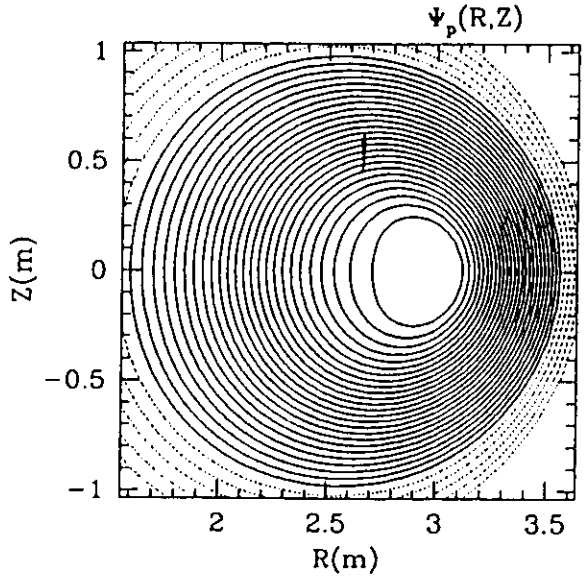

at $r/a = 0.3$, $\hat{s} = -.17$, $\Delta' = .53$

Densities $\times 0.1$

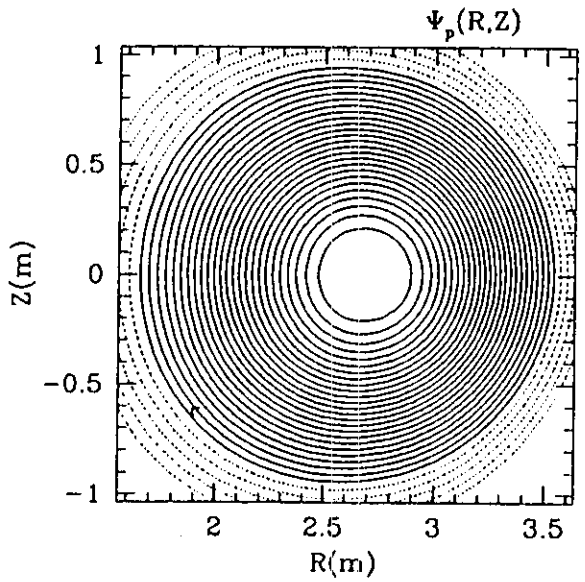

at $r/a = 0.26$, $\hat{s} = -.17$, $\Delta' = .07$

- Numerically calculate $\langle \omega_{de} \rangle_b (\kappa)$ using JSOLVER output

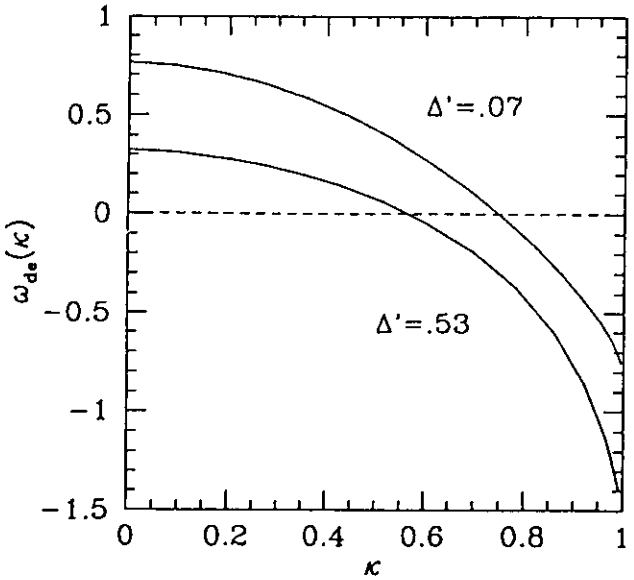

75% drift reversal at $\Delta' = .53$, 60% drift reversal at $\Delta' = .07$

Precession drift frequency at low-β, small r/R

In the low-β, small $\epsilon = r/R$ limit, the curvature and ∇B drifts are (for $\theta_0 = 0$):

$$i\omega_d \Phi = \frac{1}{B^2} \mathbf{B} \times \nabla \mathbf{B} \cdot \nabla \Phi$$

$$\omega_d \approx \cos\theta - \frac{1}{2}(\Delta' + \epsilon) - \epsilon/q + \hat{s}\epsilon/2q + \hat{s}\theta \sin\theta - r\Delta'' \sin^2\theta + \Delta' \hat{s}\theta \sin\theta \cos\theta - \hat{s} \sin^2\theta (\Delta' + \epsilon) + \mathcal{O}(\epsilon^2)$$

The $\hat{s} - \alpha$ model only keeps three of these terms

$$\alpha = -q^2 R \frac{d\beta}{dr} \propto \Delta''$$

$$\Delta' \propto \left(\frac{l_i}{2} + \beta_0 \right) r$$

and misses the reduction in precession frequency for all particles (not just deeply trapped) from Δ'.

Simple Physical Picture of Shafranov Shift Induced Drift Reversal

Since **perturbations** follow field lines, flux compression decreases k_θ in bad **curvature** region, increases k_θ in good curvature region

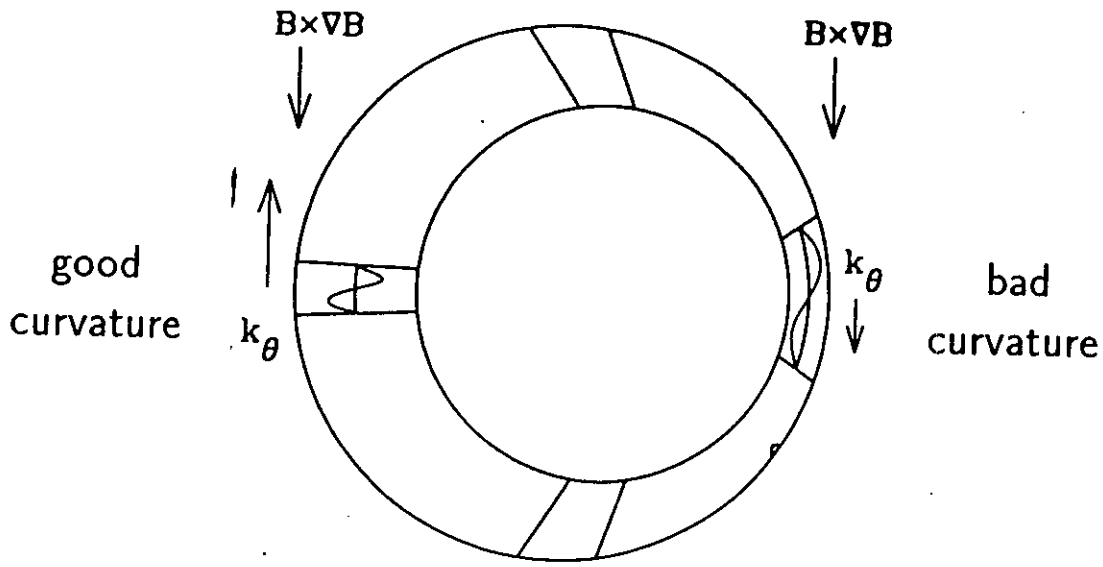

$\omega_d \propto \mathrm{B} \times \nabla \mathrm{B} \cdot \nabla$ decreases, bad curvature region shrinks

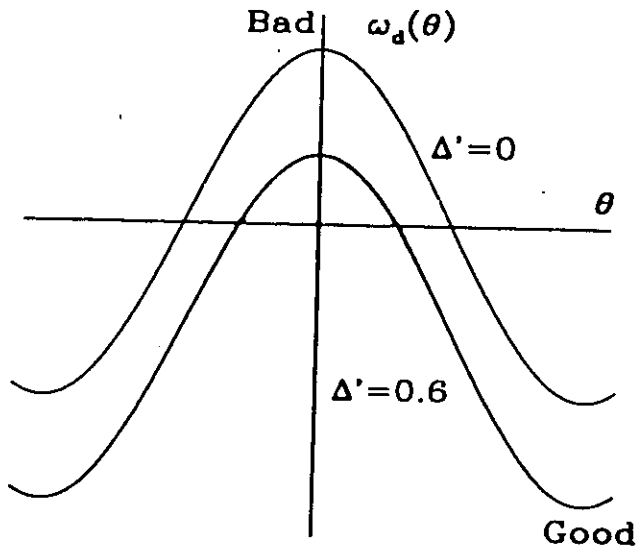

Nice picture of negative shear stabilization [Antonsen, Drake, *et al.*, 1996]

Possible ITB formation scenarios

Usually, transport increases as gradients are increased

Turbulence suppression requires transport to decrease as gradient is increased $\Rightarrow$ positive feedback

2nd stability to TEM is such a mechanism Bew et al PoP 1997

1. Stabilization of TEM from Shafranov shift is a potential positive feedback mechanism for transition

$$P_{\rm beam} \uparrow \Longrightarrow \nabla p \uparrow \Longrightarrow \Delta' \uparrow \Longrightarrow \text{transport} \downarrow$$

- OMS and ERS plasmas have unusually large Δ': both q and β are large in core

2. Radial $\mathbf{E} \times \mathbf{B}$ flow shear can be induced either by ∇p (TFTR) or $\mathbf{v}_{\rm tor}$ (TFTR back-trans, DIII-D, JET) . Waltz found stabilization when $\omega_E > \gamma$. In general geometry appropriate shearing rate is $\omega_E = (RB_p/B)d/dr(E_r/RB_p)$ [Hahm&Burrell].

$$P_{\rm beam} \uparrow \Longrightarrow \nabla p \uparrow \Longrightarrow E_r' \uparrow \Longrightarrow \text{transport} \downarrow$$

- OMS and ERS core also have large ω_E, since B_p is small, ∇p is large, and ω_E is enhanced by Δ'

$\mathbf{E} \times \mathbf{B}$ shearing rate comparable to γ at transition

Measured shearing rate $\omega_E = (RB_p/B)d/dr(E_r/RB_p)$ compared to linear growth rate for #84011 at $r = .25a$.

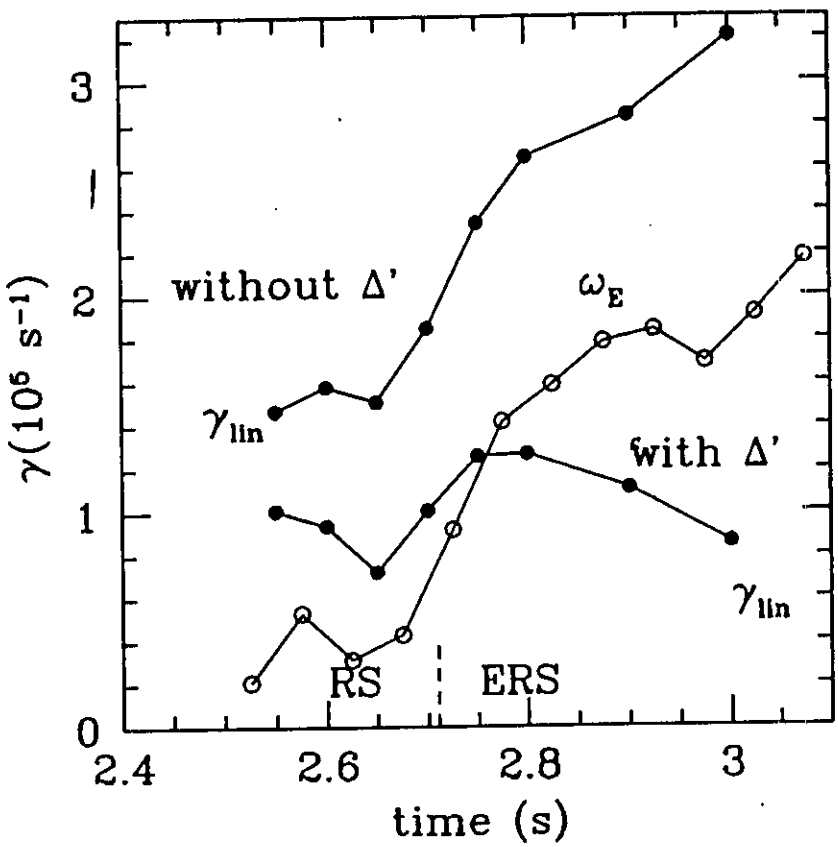

- Measured $\mathbf{E} \times \mathbf{B}$ shearing rate larger than γ after transition, $\mathbf{E} \times \mathbf{B}$ shear is probably playing a role
- Without Shafranov shift stabilization, γ_{lin} too large for $\mathbf{E} \times \mathbf{B}$ shear to stabilize

Shafranov shift can produce transition

To produce a transition, Shafranov shift stabilization must overcome increased transport from steeper density gradient.

- Starting with profiles at $t = 3$s, gradually decrease all densities
- Recompute equilibria with JSOLVER. Find $\Delta' \propto n$
- Calculate particle flux $\Gamma = -D\nabla n$ using: $D = \frac{5}{3}\left(\frac{\gamma}{k_\perp^2}\right)_{\max}$
- Within good confinement zone, $r/a = 0.3$, Shafranov shift overcomes increased gradient and causes transition
- At $r/a = 0.5$, outside good confinement zone, transport increases with increasing density, no runaway
- Core is in "second stable regime" for TEM

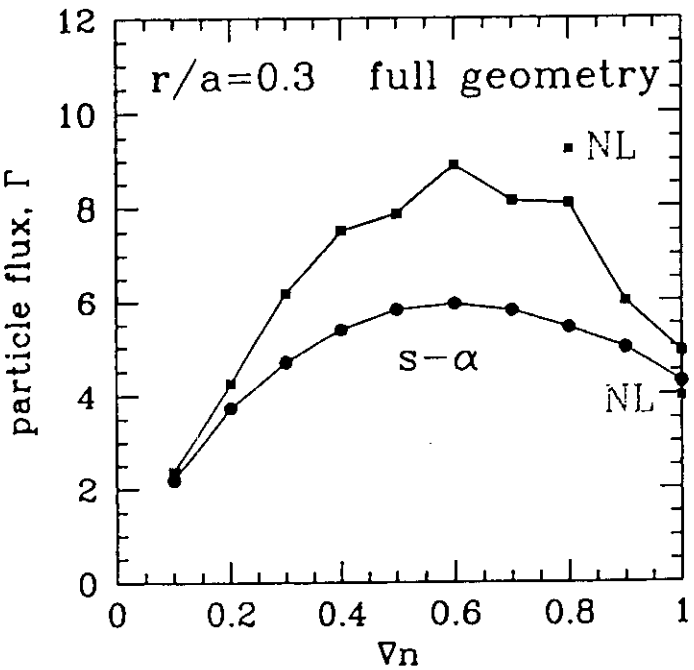

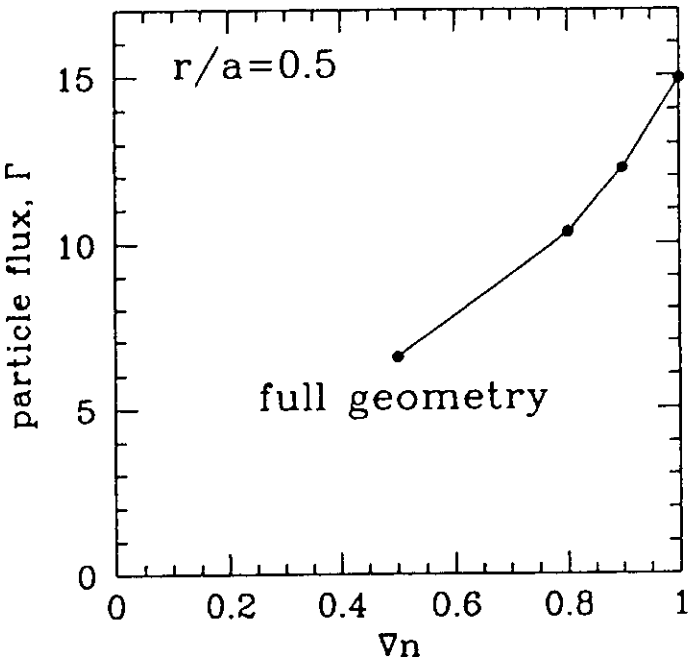

Shafranov shift stabilization can beat ∇n drive

- Reducing densities everywhere doesn't change L_n, so repeat experiment only reducing density in good confinement zone
- This increases $L_n = (\frac{1}{n_0}\frac{dn_0}{dr})^{-1}$, and reduces drive at same time Δ' is reduced

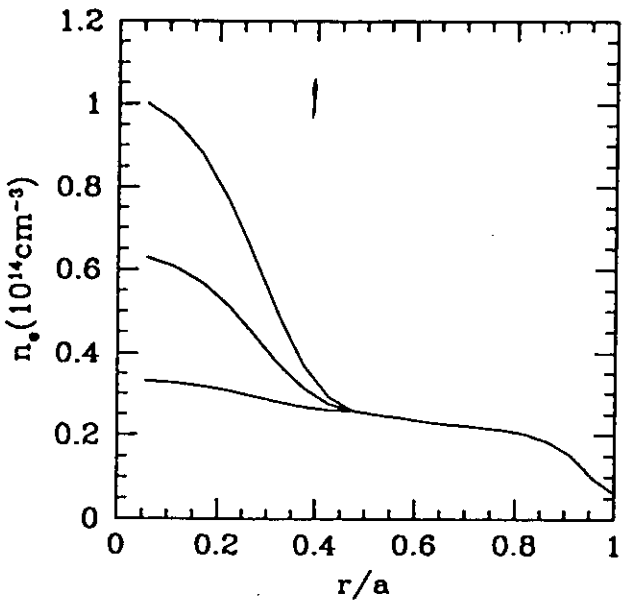

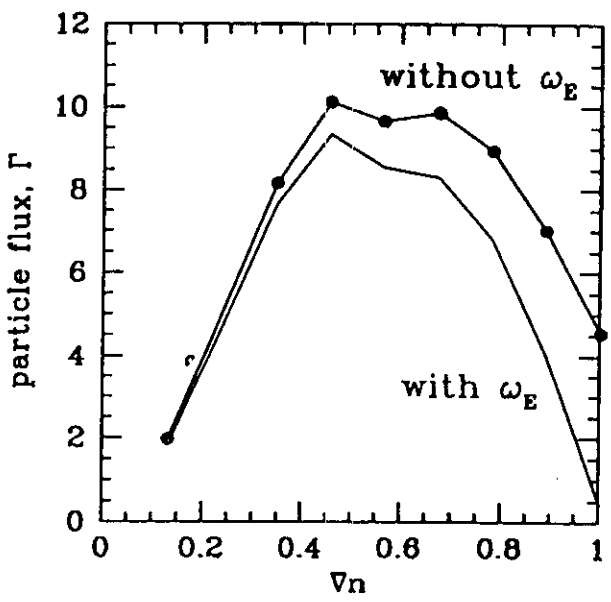

- Shafranov shift can still overcome increased drive and cause transition
- Since $\mathbf{E} \times \mathbf{B}$ shear is also $\propto \nabla n$, including ω_E will reduce threshold gradient. Δ' enhancement of ω_E included

Controlled co-ctr beam scan demonstrates that loss of E×B suppression ⇒ loss of ITB

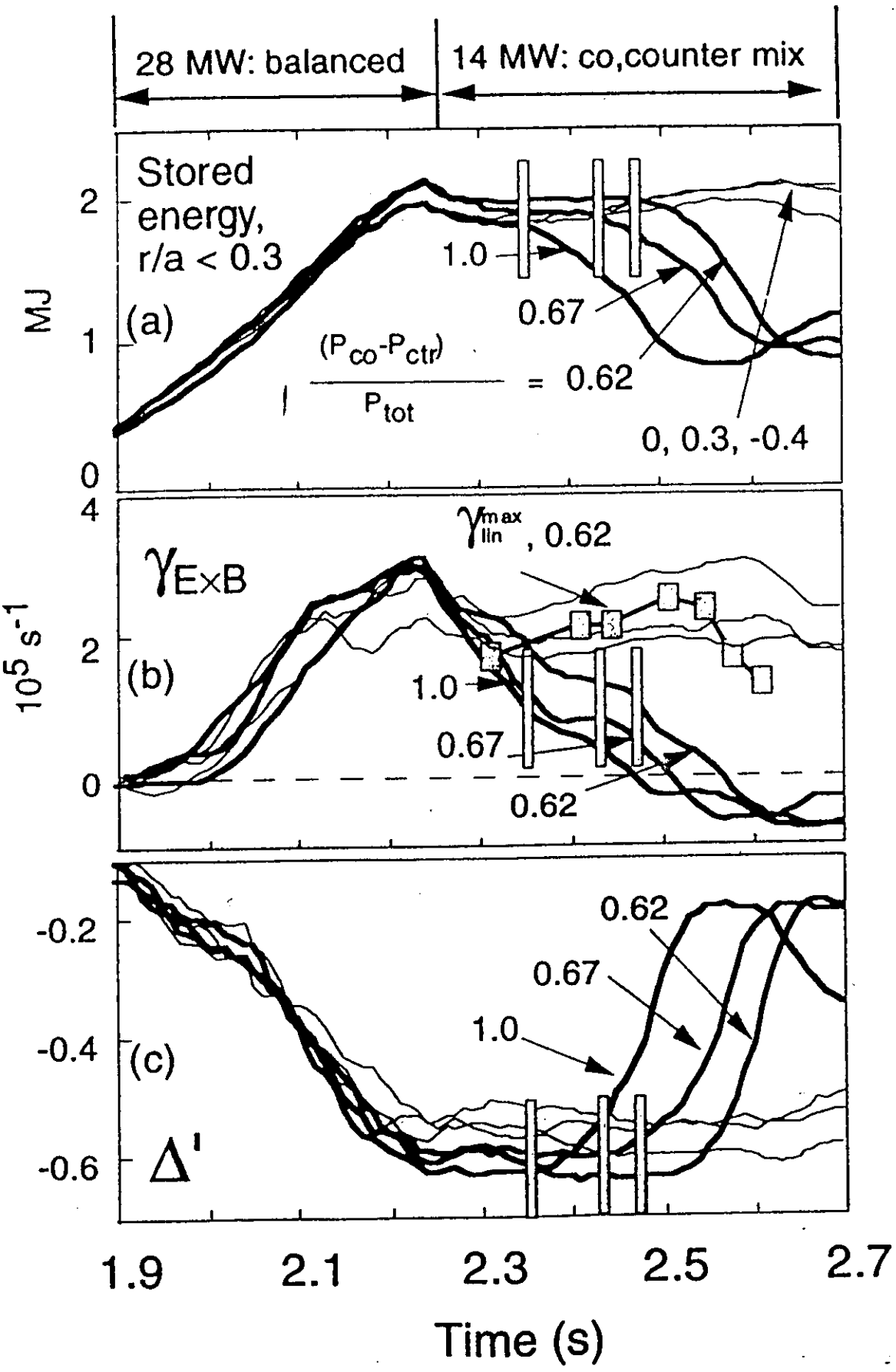

Loss of ExB suppression leads to increase in fluctuations and transport

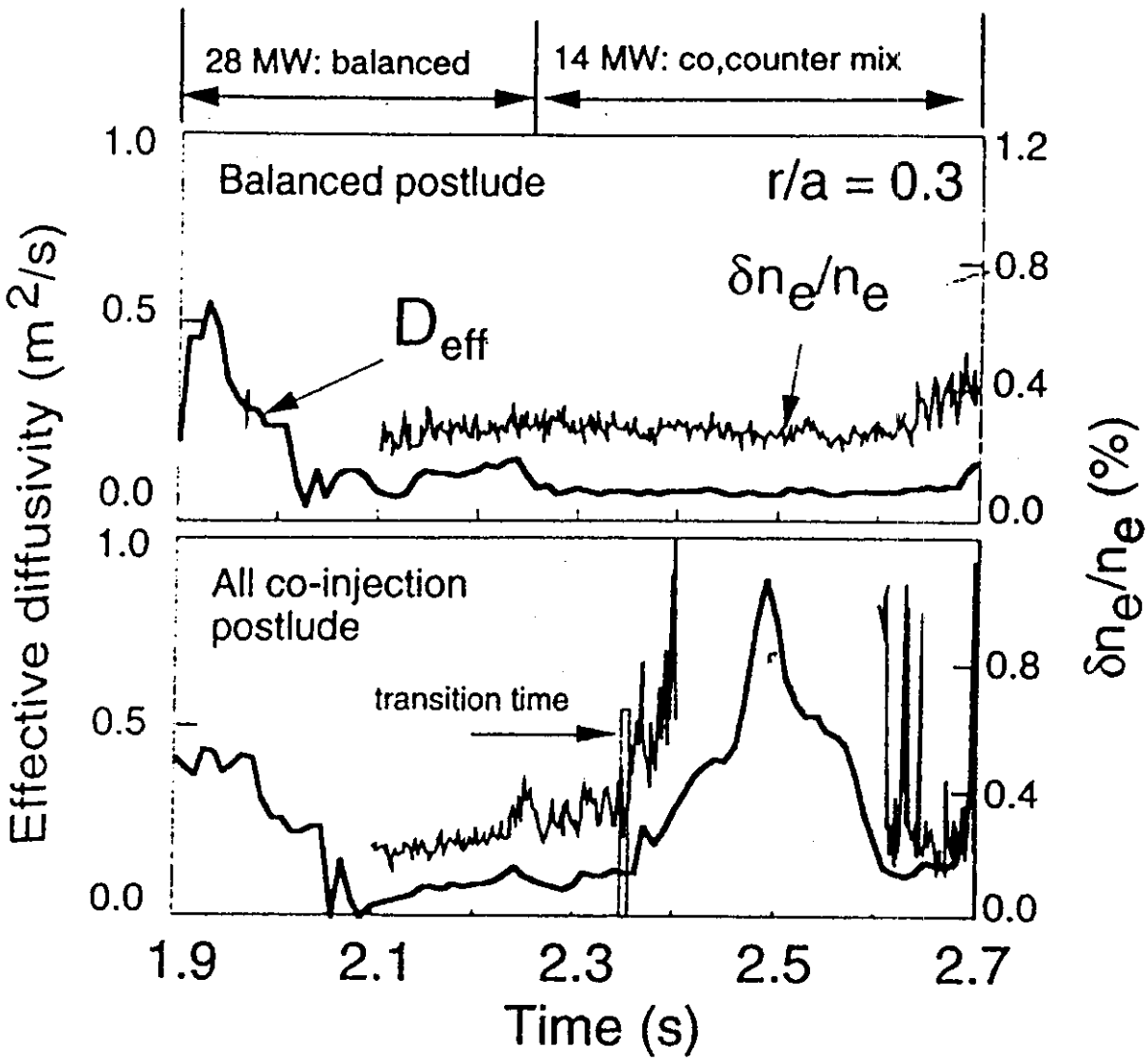

FIG. 9. The effective particle diffusivity D_{eff} and measured fluctuation amplitudes at $r/a = 0.3$ for plasmas with (a) all co-injection (b) balanced injection in the postlude.

Detailed Comparison with JET Optimized Shear

We now analyze JET optimized shear discharge 40847. Shortly after the beams turn on at $t = 5$s, an internal transport barrier forms and T_i increases sharply, and χ_i, calculated by TRANSP, drops. At $t = 6.8$s, the edge undergoes an L-H transition, and core confinement begins to deteriorate.

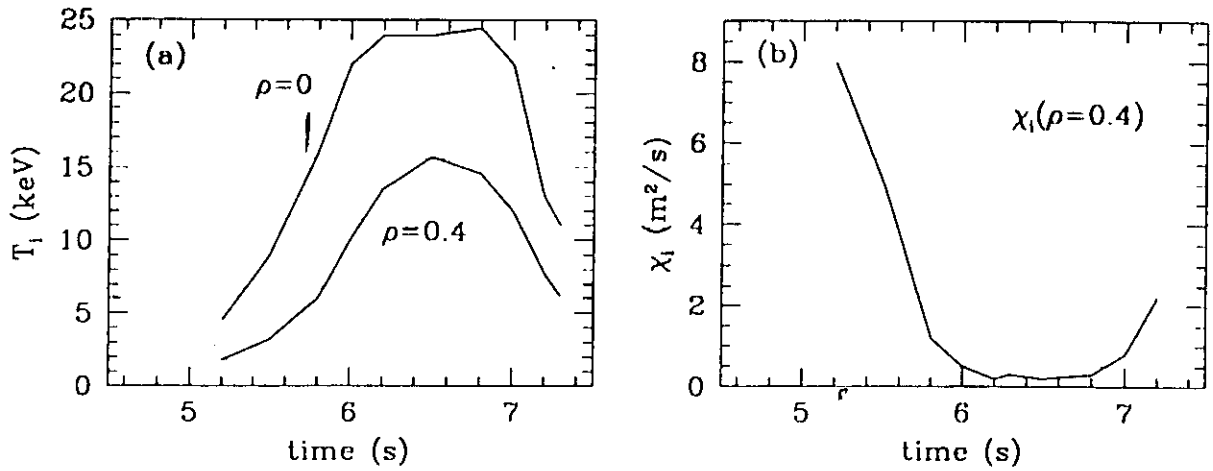

E_r is calculated from radial force balance using the NCLASS package, using measured v_ϕ and ∇p profiles and calculating the neoclassical v_θ. The contribution from v_ϕ dominates E_r. After the L-H transition, rotation slows and the shearing rate drops.

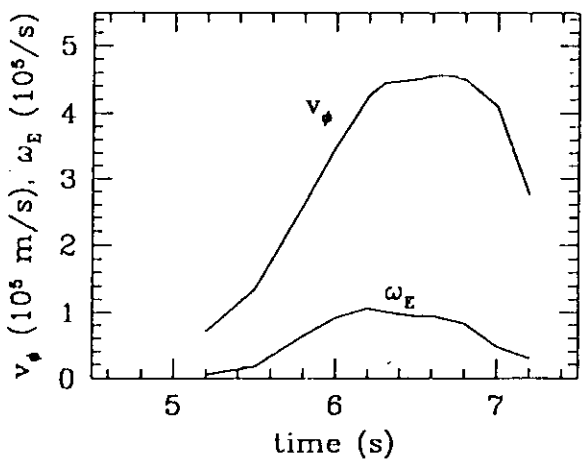

Incorporating $\mathbf{E} \times \mathbf{B}$ Sheared Flow

In each fluid equation, $\mathbf{E} \times \mathbf{B}$ convection gives rise to three terms:

$$\frac{\partial n}{\partial t} + \mathbf{v}_E^{(0)} \cdot \nabla n + \mathbf{v}_E \cdot \nabla n_0 + \mathbf{v}_E \cdot \nabla n + \cdots = 0, \qquad (1)$$

In our flux-tube simulations, we evolve $n(\alpha, \psi, \theta, t)$, where α and ψ are coordinates perpendicular to the field, $\mathbf{B} = \nabla\alpha \times \nabla\psi$, ψ is the poloidal flux, and θ measures distance along the field line. In these coordinates Eq. (1) becomes:

$$\frac{\partial n}{\partial t} - c\frac{\partial \phi^{(0)}}{\partial \psi}\frac{\partial n}{\partial \alpha} + c\frac{\partial \phi}{\partial \alpha}\frac{\partial n_0}{\partial \psi} + c\left(\frac{\partial \phi}{\partial \alpha}\frac{\partial n}{\partial \psi} - \frac{\partial \phi}{\partial \psi}\frac{\partial n}{\partial \alpha}\right) + \cdots = 0.$$

For linearly sheared $\mathbf{E}^{(0)} \times \mathbf{B}$ flow: $\frac{\partial \phi^{(0)}}{\partial \psi} = \frac{\partial^2 \phi^{(0)}}{\partial \psi^2}(\psi - \psi_0)$.

We introduce the transformation $\alpha' = \alpha - c\frac{\partial^2 \phi^{(0)}}{\partial \psi^2}(\psi - \psi_0)t$, so the new coordinates shear in the poloidal direction with the equilibrium flow. This introduces the $\mathbf{v}_E^{(0)} \cdot \nabla n$ term, consistent with smooth statistically periodic boundary conditions across the ψ domain.

Now radial derivatives become time dependent:

$$\frac{\partial}{\partial \psi} = \frac{\partial}{\partial \psi'} - c\frac{\partial^2 \phi^{(0)}}{\partial \psi^2} t \frac{\partial}{\partial \alpha}.$$

In more standard ballooning notation, this means that the θ_0's shift:

$$\theta_0' = \theta_0 + \Omega_E t/\hat{s},$$

where $k_r = k_\theta \hat{s} \theta_0$, and $\Omega_E = \frac{e}{T_i}\frac{\partial^2 \phi^{(0)}}{\partial \rho^2}$.

Linear Behavior with $\mathbf{E} \times \mathbf{B}$ Sheared Flow

In this representation the addition of flow shear introduces oscillations on top of exponential growth, and a reduced effective growth rate. $\Phi(t)$ for seven $\theta_0' s$ in the presence of $\mathbf{E} \times \mathbf{B}$ shear:

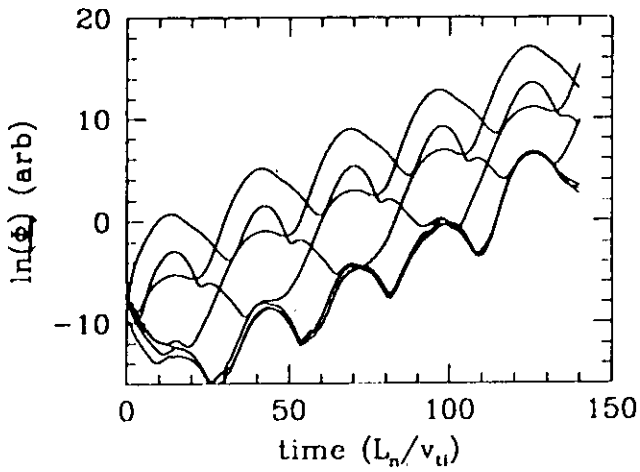

When a mode is sheared to sufficiently high θ_0, we reintroduce it at negative θ_0, to resolve the physically relevant part of k-space. Different θ_0's are linearly coupled through the boundary condition along the field line [Beer, Cowley, & Hammett, PoP 2, 2687 (1995)], making the linear calculation with flow shear 2D.

The net growth now depends on the θ_0 averaged growth rate, as a mode is convected poloidally. This approach and our results are similar to [Waltz, Dewar, & Garbet, PoP 5, 1784 (1998)]. Parallel flow shear not included.

General Geometry Treated Numerically

Calculate equilibria using JET profiles from TRANSP

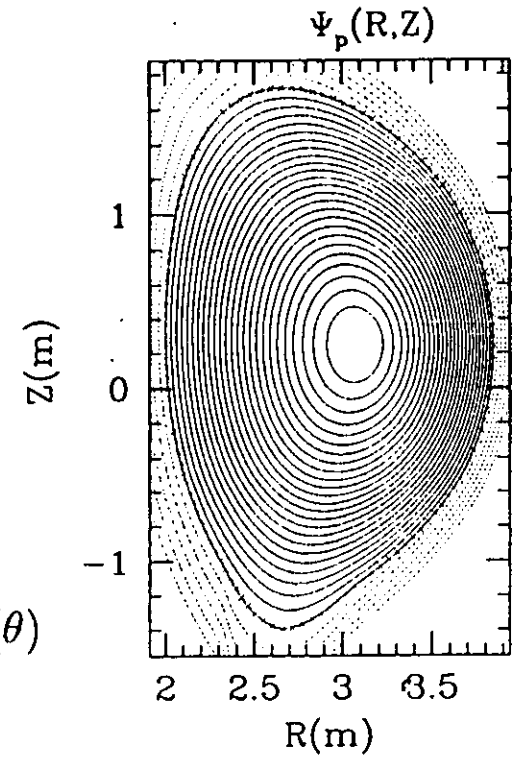

Numerically calculate $\omega_d(\theta)$ using JSOLVER output:

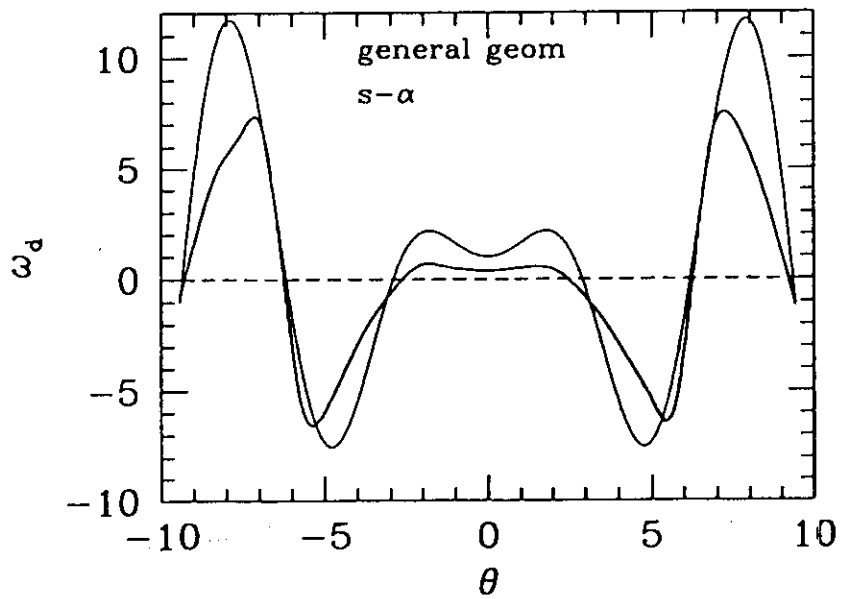

General geometry reduces bad curvature region relative to $\hat{s} - \alpha$:

$$\omega_d = \frac{k_\theta \rho_i v_{ti}}{R} \left[\cos\theta + (\hat{s}\theta - \alpha \sin\theta)\sin\theta\right]$$

Linear Results Without $\mathbf{E} \times \mathbf{B}$ Shear

Use profiles from TRANSP and their gradients as inputs at $\rho = 0.4$.

Growth rate vs. time at $\rho = 0.4$, maximized over $k_\theta \rho_i < 1.5$, ignoring $\mathbf{E} \times \mathbf{B}$ shear, labelled $\gamma_{E=0}$:

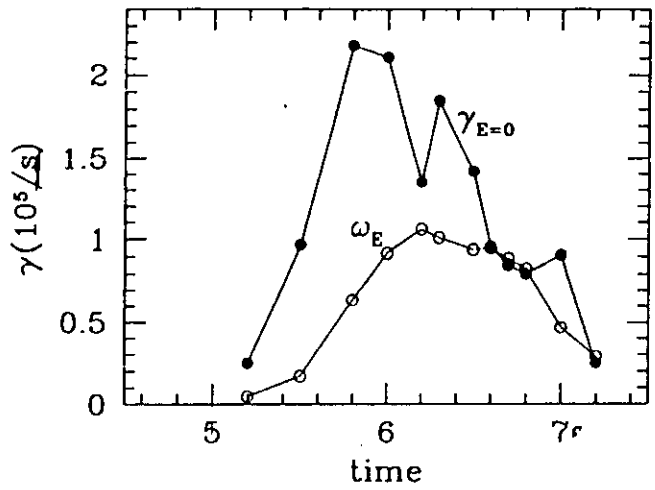

As profiles steepen, growth rates first increase and then decrease, but this does not appear to be due to geometrical finite-β stabilization [Beer, Hammett, *et al.*, PoP 4, 1792 (1997)], in contrast to ERS on TFTR. Tested by recalculating the equilibria with β reduced by 10, and repeating the growth rate calculation with new geometry but same driving gradients. Little change found.

As the growth rates drop, toroidal rotation builds up until the shearing rate, ω_E, is within a factor of 2 of $\gamma_{E=0}$. This occurs near $t = 6.2$s, roughly consistent with the decrease in χ_i.

After the L-H transition, toroidal rotation decreases until ω_E drops below $\gamma_{E=0}$ at around $t = 7$s. This is also consistent with the increase in χ_i, and the loss of the internal transport barrier.

Linear Results Including $\mathbf{E} \times \mathbf{B}$ Shear

Growth rates including $\mathbf{E} \times \mathbf{B}$ shear, labelled γ_{full}:

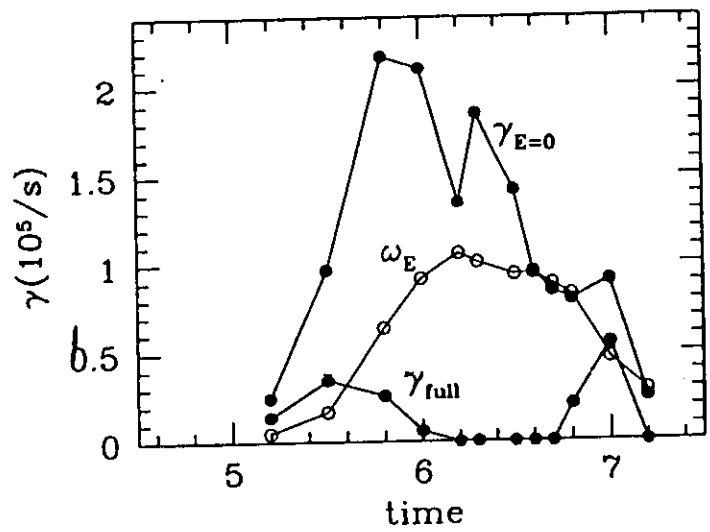

With $\mathbf{E} \times \mathbf{B}$ included, growth rates are significantly reduced, and stability is consistent with the expectation of complete linear stability when $\omega_E \sim \gamma_{E=0}$.

After $t = 6$s, we find complete stabilization, consistent with the formation of the internal transport barrier.

At $t = 6.8$s, as the shearing rate drops, complete suppression is lost, consistent with the loss of the core barrier after the L-H transition at the edge.